Computational Study of H_2 binding to MH_3 (M= Ti, V, and Cr)

James J. Hales[a], Michel L. Trudeau[b], David M. Antonelli[c], Nikolas Kaltsoyannis[a,*]

[a]School of Chemistry, University of Manchester, Oxford Road, Manchester M13 9PL, UK

[b]Materials Science, Hydro-Quebec Research Institute, 1800 Boul. Lionel-Boulet, Varennes, Quebec, J3X 1S1, Canada

[c]Department of Chemistry, Lancaster University, Lancaster, LA1 4YB, United Kingdom

Abstract

A series of amorphous materials, produced by Antonelli et al., based on hitherto elusive early transition metal hydrides MH_3 (M= Ti, V, and Cr) capable of binding H_2 via the Kubas interation, has shown great promise for hydrogen storage applications, approaching US DoE system targets in some cases, even when considerations for the system are taken into account. We here apply quantum chemical computational techniques to study these materials. Starting with monomeric MH_3 (M= Ti, V, and Cr) we progress to M_2H_6 and then penta-metallic systems as representations of the H_2 binding sites, analyzing the geometries, energies, H_2 vibrational frequencies and binding modes, finding clear evidence of significant Kubas binding. This enables these materials to bind dihydrogen with a binding energy of between 22 and 53 kJ mol^{-1}. In agreement with experiment, we conclude that while TiH_3 binds H_2 exclusively through the Kubas interaction, VH_3 and CrH_3 additionally physisorb dihydrogen, making these more attractive for practical applications.

Introduction

Hydrogen fuel cells are potential alternatives to the current fossil fuel powered engines that are detrimental to the environment[1-4]. However, the current generation of hydrogen powered vehicles makes use of carbon fibre-based high pressure cylinders that require frequent refuelling[5,6]; although hydrogen is very energy rich by weight the volume required to fuel a vehicle for long distances is prohibitive. For a driving range exceeding 500 km around 5 kg of H_2 is required; this needs a carbon fibre cylinder with a volume of around 125 L when pressurised to 700 bar[7], adding additional constraints to vehicle design. Hence a more commercially attractive and efficient solution to storing the gas is required to encourage higher rates of adoption of hydrogen powered vehicles.

Materials-based solutions have been proposed to store hydrogen in large quantities[8-10]. In general, these materials can be categorised into three groups depending on the type of interaction they have with dihydrogen. One group, which includes many MOFs, binds hydrogen through physisorption[11,12]; the interaction is weak, with a binding energy of around 10 kJ mol^{-1}, which can give promising kinetic properties but requires cryogenic temperatures, 77 K, to store significant amounts of the gas, which generates other problems. By contrast, metal hydrides[13,14] show much stronger binding interaction with H_2 (> 50 kJ mol^{-1}) which leads to greater storage capacities but at the expense of difficulties in extracting the dihydrogen for use. Both physisorption and chemisorption materials have problems with heat management as the gas either readily boils off or is difficult to release. An ideal solution should in principle arise from material–dihydrogen binding with energies between these extremes[15-17], and a third category of proposed hydrogen storage solutions does indeed meet this requirement. These materials exploit the Kubas interaction[18], in

which the H_2 σ orbital donates electronic density into a metal d orbital and concurrently a second metal d orbital donates electronic density into the H_2 σ* orbital; analogous to the bonding between d block metal centres and alkenes in the Dewar-Chatt-Duncanson model[19]. This orbital interaction produces metal-H_2 complexes characterised by a weakening and extension of the H–H bond.

In recent years there has been an increasing interest in developing materials that exploit the Kubas interaction including, from our labs, those based on hydrazines[20], hydrazides[21], doped mesoporous silica molecular sieves[22,23], and early transition metal alkyl hydride gels[24-27]. The latter have shown considerable promise as novel hydrogen storage materials; TiH_3, VH_3, and CrH_3 have hydrogen storage capacities of 3.49, 5.80, and 5.08 wt% under pressure at room temperature, with the potential to be much greater. Raman spectroscopy indicates that these materials bind H_2 *via* the Kubas interaction, although they have surprisingly low adsorption enthalpies as measured by *in situ* calorimetry considering that the hydrogen binding properties persist at room temperature. Hence to probe further the hydrogen binding properties of these materials we here look towards computational methods, which we have previously found to be very informative in understanding Kubas-based systems[27-30]. We have calculated dihydrogen binding to MH_3 monomers and dimers (M = Ti, V, Cr), as well as to more extended pentameric structures. We find extensive Kubas binding in all metal hydrides, with maximum loading levels and H-H stretching frequencies in good agreement with experiment.

Methodology

Dispersion-corrected generalised gradient approximation density functional theory (DFT) has been employed throughout this study, combining the PBE functional[31,32] with Grimme's D3 dispersion corrections[33] and the 6-311++G** basis set[34-37]. This approach has been shown by others[38,39] to provide reasonable geometry, IR and electronic data in benchmarking against *ab initio* techniques.[40-43] Both Gaussian 09 revision D.01[44] and Gaussian 16 revision A.03[45] have been used to perform the calculations presented herein; we have found that both codes produce the same outputs in test cases.

Spin unrestricted DFT was used throughout. Ti(III), V(III), and Cr(III) centres were treated with 1, 2, and 3 unpaired electrons (upe) respectively; base structures (*i.e.* the metal hydrides without added H_2) with multiple metal centres were considered to have the highest possible number of unpaired metal-based valence electrons.

No constraints were imposed during geometry optimisations, which were performed with the default settings except (i) the integration grid was increased from default to UltraFine (ii) geometry convergence criteria were tightened to a maximum force on an atom of 2×10^{-6} a.u., the root mean squared average (RMS) force to 10^{-6} a.u. on all the atoms, the maximum displacement of an atom to 6×10^{-6} a.u., and the RMS of the displacement to 4×10^{-6} a.u for each of the monomeric and dimeric systems along with the pentameric base structures. Systems with H_2 bound to the pentamers and those marked in the supplementary information were converged to at least the Gaussian default criteria, with maximum force of 4.5×10^{-4} a.u., RMS force to 3×10^{-4} a.u. on all the atoms, the maximum displacement to 1.8×10^{-3} a.u., and the RMS of the displacement to 1.2×10^{-3} a.u. Harmonic vibrational frequency analysis was performed on all optimised systems to confirm the

calculation has reached a true minimum structure with no imaginary frequencies, and to provide thermal energy corrections to the hydrogen binding energies (HBEs) to yield Gibbs energies.

Throughout this work we have used molecular representations of the H_2 binding sites. These can be broken down into the representation of the MH_3 base structure and the base structure plus bound H_2. The average HBE is calculated by taking the energy of the system loaded with dihydrogen and subtracting the energies of the base structure and the individual H_2 molecules; this is then divided by the number of dihydrogen molecules present *n* to give the average HBE:

$$HBE = \frac{1}{n}[E(Loaded\ System) - E(Base\ Structure) - nE(Dihydrogen)]$$

The distance $d_{M\text{-}H2}$ is defined as the mean of the distances from the closest metal centre to each atom in the H_2 unit.

The maximum H_2 loading on the base structures was determined through the following method: H_2 was added to the base structures incrementally until further additions had no strong interaction with the base structure. For the MH_3 monomers and dimers this point was determined by the orientation of the additional H_2; these were considered to be non Kubas binding when there are differences in the two M-H(H_2) distances greater than 0.4 Å. For the pentamers a different approach was used; the maximum loading was determined to be the point at which an added H_2 was found to be closer to another H_2 than to the base structure. This latter approach is that adopted in our recent study of H_2 binding to the Mn-based storage material KMH-1[27].

Results and Discussion

H_2 binding to monomers of MH_3 (M = Ti, V, Cr)

The initial step towards understanding the dihydrogen binding occurring in these MH_3 systems was to probe the interaction between H_2 and monomeric MH_3 (M = Ti, V, Cr). The latter are all are non-planar, although VH_3 has an H-V-H angle of 119˚ and so is approaching a trigonal planar geometry. Table 1 contains the hydrogen binding energies and key geometric data for the MH_3 systems with a single H_2 present, as well as the maximum loading level achieved for each metal hydride.

Table 1. Hydrogen Binging Energies (kJ mol^{-1}), H_2 Geometric data (Å) and Stretching Frequencies (cm^{-1}) for MH_3 (M= Ti, V, Cr)

Metal	Number of H_2 bound	Average HBE, ΔE	Average HBG, ΔG	Average $d_{H\text{-}H}$ H_2	Average $d_{M\text{-}H2}$	Stretching Frequencies
Ti	1	-36.3	5.9	0.834	1.917	3044
	5	-41.1	2.1	0.817	1.939	Table 2
V	1	-51.8	-9.2	0.810	1.839	3414
	4	-55.0	-11.2	0.829	1.850	Table 2
Cr	1	-24.1	13.8	0.786	1.973	3761
	3(4)	-48.0	-5.1	0.867	1.823	Table 2

At the SCF energy level (ΔE) each of the systems binds a single dihydrogen in a thermodynamically favourable manner, with the strongest interaction seen for V. All are within the expected range for Kubas binding (20-50 kJ mol^{-1}). The Gibbs energies of the binding (HBG) for a single H_2 is favourable only for V, and is much weaker than at the SCF level, with the other systems producing energies suggesting no binding would occur. Indeed, the Gibbs energies are all between 37.9 and 42.6 kJ mol^{-1} less favourable than the SCF energies, unsurprising given the entropic penalty of bringing together two molecules to form one.

The bond length in an isolated H_2 molecule is calculated to be 0.752 Å. All the H-H distances in Table 1 are significantly longer than this; a hallmark of the Kubas interaction.

The largest extension (0.082 Å) is seen for a single H_2 bound to TiH_3, clearly within the range proposed by Kubas (0.05-0.25 Å). However, this lengthening does not correlate well (R^2 = 0.19) with the HBEs as V, the metal which generates the strongest H_2 binding, leads to an H-H bond extension of only 0.058 Å. The geometric feature which best correlates (R^2 = 1.00) with the binding energies is the distance from the metal centre to the H_2 unit; V holds H_2 the closest followed by Ti then Cr. The stretching frequency of the bound H_2 correlates inversely and perfectly (R^2 = 1.00) with $d_{H\text{-}H}$ H_2 for the singly loaded systems.

H_2 binding induces only minor changes in the geometries of the MH_3 structures; in all cases when H_2 is added the symmetry reduces from C_{3V} to C_s. For the Ti system, figure 1A, there is a less than 1% extension in the Ti-H bonds. The 2-1-4 and 3-1-4 H-Ti-H angles are slightly contracted, by 2.5%, and the other H-Ti-H angle, 2-1-3, is expanded by 1.1%. The V system, figure 1B, shows slightly different behaviour; the V-H bonds are contracted by <1% and the 2-1-3 and 4-1-3 H-V-H angles are contracted, by 3.2%, whereas 2-1-4 is expanded by 2.2%. The Cr system, figure 1C, shows the most significant change as the Cr-H bond length, 1-3 is extended by 1% and the other bond lengths extend by <1%; the H-Cr-H angle, 2-1-4, increases by 6.3% and the other two are contracted by 2.8%.

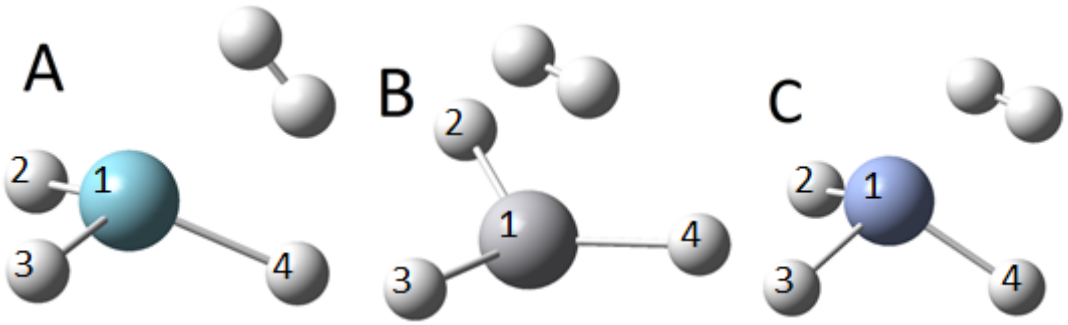

Figure 1. Ball and stick representations of a single H_2 binding to the MH_3 monomers. A = TiH_3, B = VH_3 and C = CrH_3.

In order to verify the presence of the Kubas interaction, we have analysed the molecular structure of the H_2 bound systems. The Kohn-Sham molecular orbitals that contribute to the bonding between H_2 and VH_3 are shown in figure 2; the pertinent orbitals for Ti and Cr can be found in the supplementary information figures S1 and S2. There are two orbitals, HOMO-1 and HOMO-3, that show back bonding in which a metal d-orbital interacts with the H_2 σ* orbital and a third molecular orbital, HOMO-5, which shows the donation from the H_2 σ orbital into another metal d-orbital.

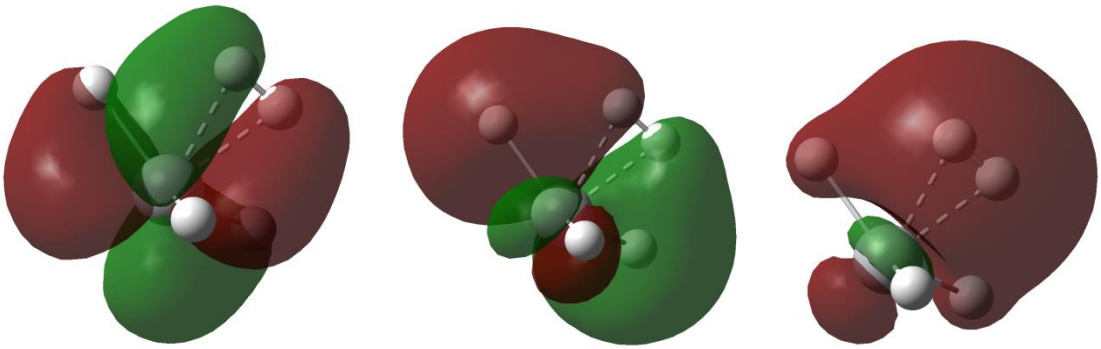

Figure 2. The orbitals involved in the binding of H_2 to VH_3. Left: HOMO-1, Centre: HOMO-3, and Right: HOMO-5. Isovalue = 0.02 a.u.

Ball and stick representations of the maximally loaded MH_3 systems are shown in figure 3. At the maximum loading level, the VH_3 and CrH_3 units are now planar, C_{2v}, with two co-planar H_2 units and the remaining H_2 in "axial" positions. TiH_3 remains non-planar, C_s; at its maximum loading the hydrides are in plane with each other, and the H_2 units are arranged all around the central TiH_3 structure. The maximum H_2 loading decreases from five for TiH_3 to four for VH_3 and three/four on CrH_3. The geometry of CrH_3 changes very significantly as the H_2 loading is increased; most notably, at the maximum loading, two of the hydrides come together to an H-H distance of 0.917 Å, which is within the range that can be considered as dihydrogen complexation, and so we view the final structure as having

three added H_2 with another H_2 coming from the base structure itself. The average HBE at the SCF level is greater for all three systems when at a maximum loading than for their singly loaded counterparts, with the greatest change seen for the Cr system. The increase in HBE is such that even at the Gibbs level both the V and Cr systems show weakly favourable binding, although ΔG for $TiH_3/5H_2$ is still very slightly positive (probably because complexation involves the greatest reduction in the number of molecules in this system); the change from SCF to Gibbs level is, again, around 40 kJ mol^{-1}.

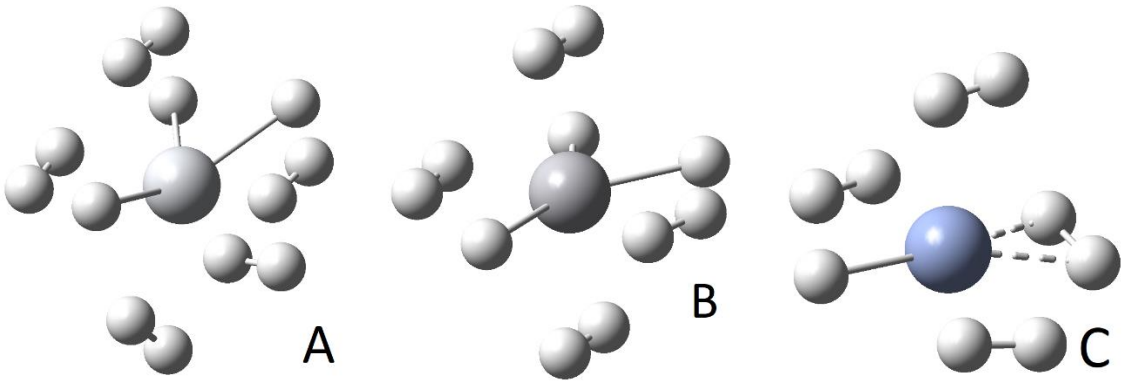

Figure 3. Ball and stick representations of the maximum loading on the MH_3 monomers. A = TiH_3, B = VH_3 and C = CrH_3. The dashed lines in C indicate the change in the base structure to form a dihydrogen unit.

As with the single H_2 case, the average extension of the H_2 bond distances (Table 1) in the maximally loaded systems does not correlate (R^2 = 0.05) with stronger binding, as for maximum loading the Cr system has the greatest average $d_{H\text{-}H}$ increase but is not the most strongly binding. There is no longer a strong correlation between the average HBE and the average distance from the metal centre to each H_2 (R^2 = 0.53) although a modest inverse correlation (R^2 = 0.69) is now seen between $d_{H\text{-}H}$ and $d_{M\text{-}H2}$ that is not present in the singly loaded cases.

The bond lengths and associated stretching frequencies for each H_2 on MH_3 at the maximum loading level are given in table 2. The correlation between these two metrics is essentially perfect in all cases. For the V system there are two pairs of H_2; the H_2 co-planar with the base structure are the most extended with the lowest stretching frequencies. The two H_2 in the Cr system which have the same bond length are both ones introduced to the base structure, and do not come from changes in the geometry of the base structure upon H_2 loading.

Table 2. Individual H-H Bond Distances (Å) and Stretching Frequencies (cm^{-1}) for the Maximum Loadings of H_2 on MH_3 (M=Ti, V, and Cr). R^2 data are for the correlation of these two variables.

	d_{H-H} H_2	Stretching Frequency	R^2		d_{H-H} H_2	Stretching Frequency	R^2		d_{H-H} H_2	Stretching Frequency	R^2
	0.834	3077			0.861	2782			0.917	2291	
	0.831	3122			0.861	2797			0.889	2530	
Ti	0.813	3335	0.99	V	0.797	3586	1.00	Cr	0.889	2547	1.00
	0.810	3387			0.797	3604			0.774	3936	
	0.799	3570									

While the monomeric model shows that in principle MH_3 can form complexes with H_2, the experimental data[24-26] suggest that these compounds are extended, networked hydrides. It is therefore of interest to explore what happens when these binding sites are part of larger systems, and the next step in our study was to probe the effect of a second metal centre on the binding characteristics. This approach to find more realistic binding sites for H_2 on transition metal hydrides has been used in our recent study of MnH_2 and its hydrogen storage properties[27].

H_2 binding to M_2H_6 (M = Ti, V, Cr)

The dimeric base structures are shown in figure 4. They are quite similar to one another with three terminal hydrides and three bridging hydrides. The Ti structure has no mirror plane as the two terminal hydrides that share a metal centre are offset from the Ti-Ti axis. The other two structures have mirror planes through the terminal hydrides and the metals. In the Cr system the terminal hydrides that share a metal are much closer together than for the other two systems.

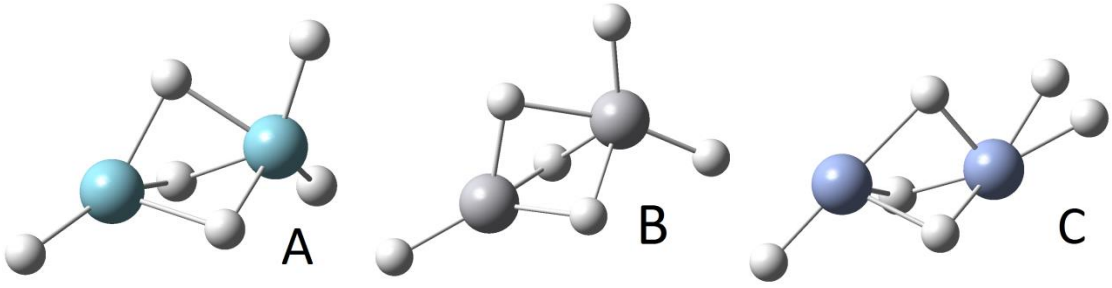

Figure 4. Ball and stick representations of the base structure representations of the MH_3 dimers. A = Ti_2H_6, B = V_2H_6 and C = Cr_2H_3.

Table 3 contains the hydrogen binding energies and key geometric data for the M_2H_6 systems with a single H_2 present, as well as the maximum loading level achieved for each metal hydride dimer. At the single H_2 loading level the binding energies are larger than those seen on the monomeric systems. For the M_2H_6 systems Cr is the strongest binding at a single loading with V being the weakest; different from that seen for MH_3. Interestingly, in Cr_2H_6 a dihydrogen unit is formed from the base structure when a second H_2 is introduced, figure 5. This is similar to the maximum loading case for CrH_3, although now only one additional H_2 is needed to induce this change. As before, the Gibbs energies are much lower, by around 50 kJ mol^{-1}, than the SCF (ΔE) energies although in all cases the HBG are negative, unlike for the smaller model.

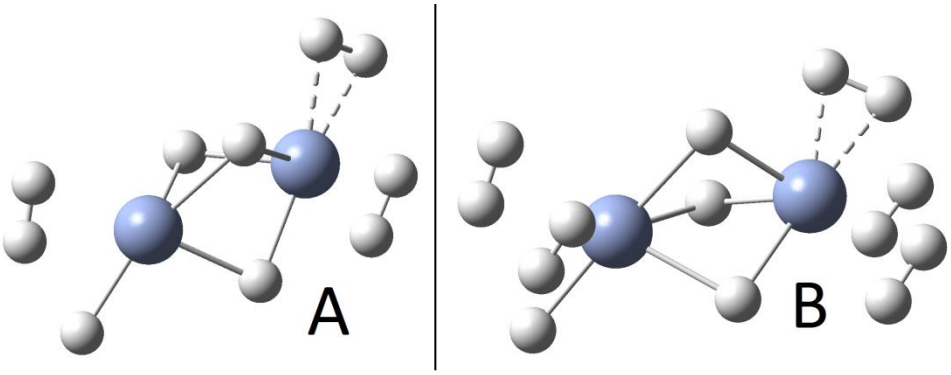

Figure 5. Ball and stick representations of the CrH_3 dimers at various H_2 loading levels. A = $Cr_2H_3.2H_2$, B= $Cr_2H_3.4H_2$.The dashed lines indicate the change in the base structure to form a dihydrogen unit.

Table 3. Hydrogen Binging Energies (kJ mol^{-1}), H_2 Geometric data (Å) and Stretching Frequencies (cm^{-1}) for M_2H_6 (M = Ti, V, Cr)

Metal	Number of H_2	Average HBE, ΔE	Average HBG, ΔG	Average d_{H-H} H_2	Average d_{M-H2}	Stretching Frequencies
Ti	1	-83.7	-34.6	0.822	1.928	3229
	6	-51.7	-7.1	0.822	1.946	Table 4.
V	1	-71.0	-21.7	0.872	1.776	2671
	5	-57.5	-13.0	0.818	1.865	Table 4.
Cr	1(2)	-97.9	-50.2	0.892 (0.903, 0.881)	1.725	2405, 2595
	4(5)	-50.6	-9.4	0.825	1.871	Table 4.

As before, the complexed H_2 bonds are significantly extended, especially for the V and Cr systems where the extension is more than 0.1 Å with a single H_2 present. The two geometry metrics given in table 3 correlate perfectly (R^2 = 1.00) *i.e.* as the H_2 move further from the metal centre they are less extended. Neither metric correlates with HBE; for d_{H-H} R^2 = 0.09 and for d_{M-H2} R^2 = 0.07. The H_2 stretching frequencies correlate perfectly with the lengthening of the bonds (R^2 = 1.00).

The amount of H_2 was increased to the maximum loading which maintains the orientation required for Kubas orbital interaction; however for Cr, as noted above, an additional H_2 is formed from the base structure upon addition of H_2, figure 5. As the amount of bound H_2 is increased the HBE falls significantly; this is by contrast to the monomeric

systems but consistent with earlier studies,[27] with all the metals giving final average HBEs between 50 and 60 kJ mol^{-1}. The strength of binding follows the order V > Cr > Ti, with V now binding most strongly, by contrast to when only a single H_2 is added; at the Gibbs level the trend is maintained.

The bond lengths and associated stretching frequencies of each H_2 on M_2H_6 at the maximum loading level are given in table 4. The H_2 bonds are extended in each system suggesting complexation through the Kubas interaction. For each M_2H_6 the stretching frequency of H_2 is correlated with the distance between H_2 and its closest metal centre, and the H-H bond length is inversely correlated with both of them; R^2 values can be found in table 4. Unexpectedly, the average extension in H_2 bond length and average distance from the closest metal centre to each H_2 are not correlated for the dimer at the maximum loading level (R^2 = 0.03). The relationship between average bond length and average HBE is now almost linear for $d_{H\text{-}H}$ (R^2 = 0.93), as expected the more energetically favoured interactions are linked with longer H-H bonds. There is very little correlation between the average HBE and average $d_{M\text{-}H2}$ (R^2 = 0.19).

Table 4. Individual H-H bond distances (Å) and stretching frequencies (cm^{-1}) for the maximum loadings of H_2 on M_2H_6 (M=Ti, V, and Cr). R^2 values for correlation between $d_{H\text{-}H}$ and $d_{M\text{-}H2}$, $d_{H\text{-}H}$ and stretching frequency, and $d_{M\text{-}H2}$ and stretching frequency are given in this order. Ti: 0.78, 1.00, and 0.80. V: 1.00, 1.00, and 1.00. Cr: 0.91, 1.00, and 0.94.

	$d_{H\text{-}H}$ H_2	$d_{M\text{-}H2}$	Stretching Frequency		$d_{H\text{-}H}$ H_2	$d_{M\text{-}H2}$	Stretching Frequency		$d_{H\text{-}H}$ H_2	$d_{M\text{-}H2}$	Stretching Frequency
Ti	0.852	1.912	2855	V	0.832	1.827	3123	Cr	0.875	1.732	2643
	0.833	1.910	3087		0.826	1.839	3204		0.865	1.752	2734
	0.824	1.932	3207		0.826	1.839	3206		0.807	1.888	3440
	0.819	1.935	3263		0.810	1.883	3413		0.799	1.912	3539
	0.813	1.951	3350		0.794	1.936	3635		0.779	2.071	3850
	0.793	2.034	3619								
Avg.	0.822	1.946		Avg.	0.818	1.865		Avg.	0.825	1.871	

H_2 binding to M_5H_{15} (M = Ti, V) and Cr_5H_{11}

The systems discussed thus far show that the early transition metal hydrides can interact with H_2 in a Kubas like fashion to produce dihydrogen complexes. We now progress to larger metal hydride networks, specifically those containing five metals, chosen in part as this is the system size we used in our previous study of H_2 binding to a Mn hydride.

Representations of the pentameric base structures are given in figure 6. All of the structures are networks of mainly bridging and some terminal hydrides. The Ti base structure has five terminal hydrides, two of which are located on the same metal centre. V_5H_{15} has a similar structure to that of Ti_5H_{15} with five terminal hydrides. However, performing a geometry optimisation of Cr_5H_{15} yields the structure shown in figure 6C; two H_2 units are generated, similar to the CrH_3 and Cr_2H_6 structures discussed above, and we take the Cr base structure with five metal centres to be Cr_5H_{11}, figure 6D. H_2 binding calculations are performed on this revised base structure.

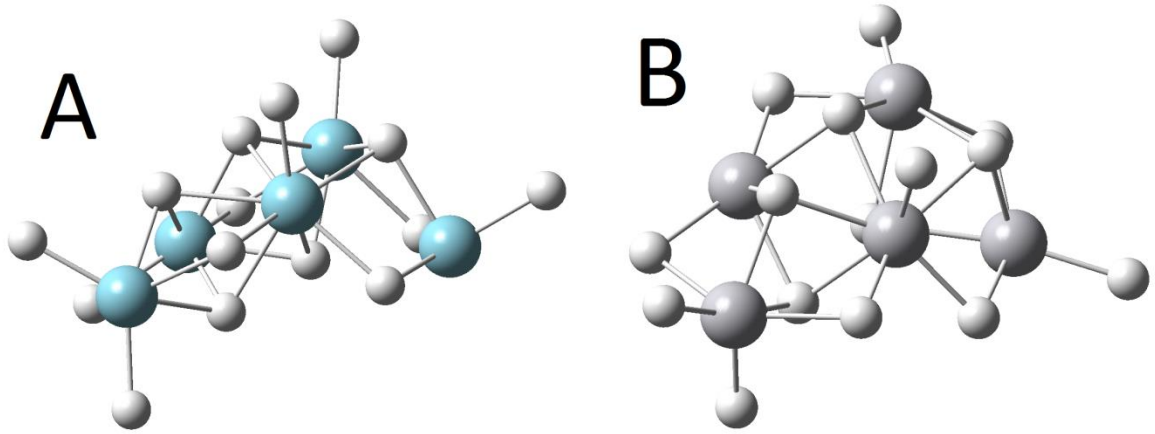

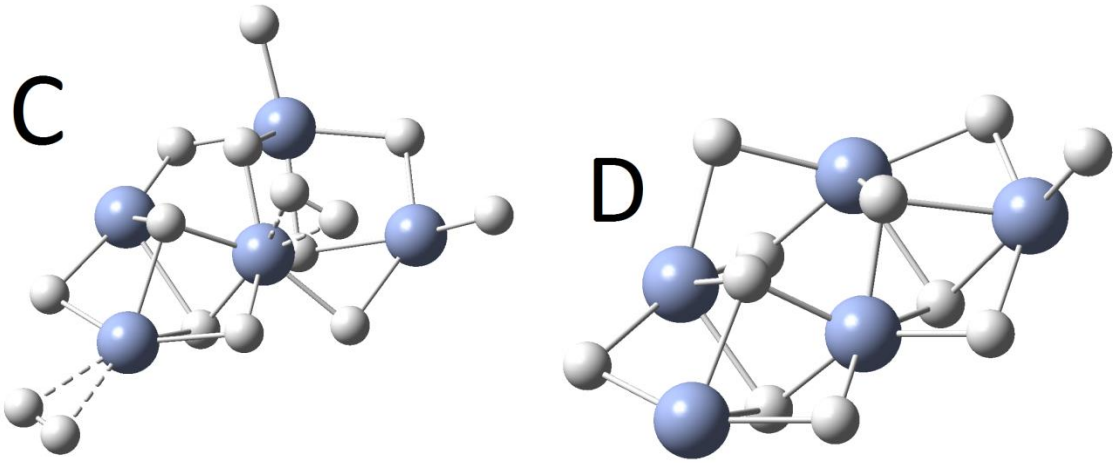

Figure 6. Ball and stick representations of A = Ti_5H_{15}, B = V_5H_{15}, C = Cr_5H_{15} and D=Cr_5H_{11}. Dashed lines show the H_2 units formed from the base structure.

Each system was investigated at loading levels of 1 H_2 per M and 2 H_2 per M. The maximum loading level was then established as discussed in the Methodology. Then, the maximum loading in which the H_2 bind predominantly to the metal centres was determined by removing any H_2 that bind closest to the hydrides; this yields the maximum number of H_2 which bind in a Kubas manner with the base structure, i.e. we distinguish physisorbed H_2 from Kubas-bound H_2. The data obtained for each of these loading levels on the five-metal centre systems are collected in table 5.

Table 5. Hydrogen Binding Energies (kJ mol^{-1}) and H_2 Geometries (Å) for M_5H_{15} (M= Ti, V) and Cr_5H_{11}

Metal	Number of H_2	Average HBE, ΔE	Average HBG, ΔG	Average $d_{H\text{-}H}$ H_2	Average $d_{M\text{-}H2}$
Ti	5	-43.1	-1.9	0.809	1.991
	10	-34.1	6.1	0.805	2.156
	Maximum Bound to Metal Centres:9	-37.1	4.8	0.811	1.982
	Maximum Bound to Base Structure:15	-25.0	9.5	0.788	2.770
V	5	-53.6	-11.1	0.842	1.857
	10	-32.9	4.7	0.805	2.389
	Maximum Bound to Metal Centres:7	-44.6	-1.3	0.832	1.852
	Maximum Bound to Base Structure:13	-26.8	7.8	0.793	2.712
Cr	5	-46.0	-2.8	0.850	1.776

10	-25.5	6.6	0.802	2.695
Maximum Bound to Metal Centres:5	As Above			
Maximum Bound to Base Structure:12	-22.6	9.1	0.793	2.690

Ti_5H_{15} with 1 H_2 per metal centre binds more strongly to H_2 than the analogous TiH_3 monomer (Table 1) with an average HBE of 43.1 kJ mol^{-1}; at the Gibbs level the H_2 binding is maintained, unlike in the monomer, but it is now very weak. The HBE suggests that the first H_2 per metal centre undergoes a Kubas like orbital interaction with Ti; the extension of d_{H-H} H_2 by 0.057 Å is also evidence of this interaction, although this lengthening is smaller than for the analogous MH_3 system. Moving to two H_2 per metal centre reduces the average HBE by 9.0 kJ mol^{-1} and becomes non-binding at the Gibbs level; the average extension of the H_2 units is slightly reduced.

Table 6 shows the bond lengths, distances from the closest metal centre, and stretching frequency for each dihydrogen in these systems. The final entry for 10 H_2 on Ti_5H_{15} is distinctly different as it is much further away from its nearest metal centre, has almost no extension in the H-H bond compared with free H_2, and has a much higher stretching frequency; these factors point to this H_2 being bound in a physisorbed fashion rather than through the Kubas orbital interaction. This physisorbed H_2 is the one that is removed to establish the maximum loading in which the H_2 bind predominantly to the metal centres (Table 5), discussed above. The maximum loading including physisorption, *i.e.* the maximum loading of H_2 to the whole base structure, not just to the metal centres, is 15; this system has a much reduced average HBE and smaller average d_{H-H} extension as only a subset of the H_2 bind in a Kubas manner. A more detailed breakdown of the H_2 geometries can be found Table S1, which shows the 9 H_2 bound in a Kubas fashion and the 6 physisorbed H_2.

Table 6. Individual H-H Bond Distances (Å) and Stretching Frequencies (ν, cm^{-1}) for the Maximum Kubas-like Loadings of

H_2 on M_5H_{15} (M=Ti, and V) and Cr_5H_{11}. Data for maximum bound to base structure can be found in the supplementary information.

Ti_5H_{15} + nH_2	d_{H-H} H_2	d_{M-H2}	Stretching Frequency	V_5H_{15} + nH_2	d_{H-H} H_2	d_{M-H2}	Stretching Frequency	Cr_5H_{11} + nH_2	d_{H-H} H_2	d_{M-H2}	Stretching Frequency
	0.858	1.867	2798		0.933	1.737	2169		0.877	1.755	2625
	0.818	1.958	3258		0.849	1.817	2907		0.877	1.722	2633
5	0.807	2.011	3404	5	0.845	1.831	2955	5	0.877	1.722	2646
	0.785	2.043	3748		0.798	1.916	3578		0.813	1.822	3350
	0.778	2.075	3884		0.787	1.982	3741		0.805	1.859	3461
R^2	d_{H-H} and d_{M-H2}: 0.98	d_{H-H} and v: 0.99	d_{M-H2} and v: 0.97	R^2	d_{H-H} and d_{M-H2}: 0.90	d_{H-H} and v: 0.98	d_{M-H2} and v: 0.96	R^2	d_{H-H} and d_{M-H2}: 0.93	d_{H-H} and v: 1.00	d_{M-H2} and v: 0.93
	0.846	1.901	2921		0.868	1.782	2721		0.877	1.755	2625
	0.846	1.890	2926		0.853	1.820	2852		0.877	1.722	2632
	0.839	1.918	3008		0.833	1.863	3081		0.877	1.722	2645
	0.812	1.968	3355		0.826	1.843	3195		0.813	1.822	3351
10	0.806	1.974	3439	10	0.815	1.846	3333	10	0.805	1.859	3461
	0.799	1.999	3544		0.800	1.913	3541		0.754	3.289	4240
	0.788	2.050	3697		0.795	1.927	3611		0.754	3.371	4243
	0.781	2.067	3824		0.755	3.456	4188		0.754	3.259	4245
	0.779	2.069	3866		0.754	3.737	4221		0.753	4.103	4260
	0.755	3.720	4204		0.754	3.703	4230		0.753	4.047	4263
R^2	d_{H-H} and d_{M-H2}: 0.44	d_{H-H} and v: 1.00	d_{M-H2} and v: 0.46	R^2	d_{H-H} and d_{M-H2}: 0.76	d_{H-H} and v: 1.00	d_{M-H2} and v: 0.80	R^2	d_{H-H} and d_{M-H2}: 0.77	d_{H-H} and v: 1.00	d_{M-H2} and v: 0.82
	0.846	1.901	2921		0.890	1.778	2489				
	0.846	1.890	2926		0.861	1.789	2793				
	0.839	1.918	3008		0.831	1.835	3138				
	0.812	1.968	3355		0.826	1.869	3168				
9	0.806	1.974	3439	7	0.820	1.841	3274	5		As Above	
	0.799	1.999	3544		0.801	1.914	3529				
	0.788	2.050	3696		0.794	1.940	3641				
	0.781	2.067	3823								
	0.779	2.069	3866								
R^2	d_{H-H} and d_{M-H2}: 0.97	d_{H-H} and v: 1.00	d_{M-H2} and v: 0.98	R^2	d_{H-H} and d_{M-H2}: 0.87	d_{H-H} and v: 0.99	d_{M-H2} and v: 0.90				

When the V system is extended to include 5 metal centres the HBE for 1 H_2 per metal centre increases from the analogous VH_3 system by 1.8 kJ mol^{-1}, and significant binding is still maintained at the Gibbs level. The extension of the H-H bond is also greater than that seen for the VH_3 analogue, 0.810 *vs* 0.842 Å; both of these metrics suggest that the complexation of H_2 is more favoured on the extended system. When the loading is increased to 2 H_2 per metal centre the HBE drops significantly and the average H_2 extension

is reduced; this is because there are 3 physisorbed H_2 present. When these are removed the average HBE increases by 11.7 kJ mol^{-1} and the bond extension is increased to only 0.010 Å less than the 1 H_2 per V system. Including physisorption, the maximum loading is 13 H_2, Table S1, with 7 Kubas-bound H_2 and 6 H_2 bound via physisorption.

When compared to the CrH_3 monomer, the binding for 1 H_2 per Cr metal centre shows a large increase in HBE. There is a corresponding large increase in the H-H bond extension for the Cr_5H_{11} system; both metrics indicate stronger Kubas orbital interactions. When an extra H_2 is introduced per metal centre there is a dramatic decrease in the average HBE to about half that at the single H_2 loading level, along with a corresponding change in H_2 $d_{H\text{-}H}$. This large change is because the second 5 H_2 all bind to the base structure *via* physisorption, *i.e.* the maximum binding to the metal centres *via* the Kubas mechanism is only 5 H_2 for this structure. The maximum loading is 12 H_2 when allowing physisorption, Table S1. More specifically, 6 H_2 bind *via* physisorption with the final H_2 bound in a fashion in between Kubas and physisorption; its bond length is lengthened *vs* free H_2, but not to the extent of the 5 Kubas H_2. When the physisorbed H_2 are included, the average the HBE is lower than for the completely Kubas binding system (with 5 H_2), as expected.

In summary, the pentameric Ti system is able to bind the most H_2 through the Kubas mechanism, 9; across the series through V to Cr the maximum amount of Kubas-like H_2 decreases by 2 per element. Each system can bind an additional 6 physisorbed H_2, and Cr_5H_{11} adds a further H_2 with weak Kubas characteristics, minor extension of the H-H bond and a stretching frequency between Kubas like binding and physisorption. V_5H_{15} binds H_2 most strongly.

Figures 7 and 8 show how $d_{H\text{-}H}$ H_2 correlates with the distance from the metal centre to each H_2, and with the stretching frequencies of H_2 respectively. The former correlation is

reasonable, R^2 = 0.75, when considering only the Kubas-bound H_2. The remaining physiosorbed hydrogen behave differently and cluster together at the left of figure 7. The relationship between $d_{H\text{-}H}$ H_2 and the stretching frequencies, shown in figure 8, is linear with an R^2 value of 0.99, suggesting that these two factors are indeed very strongly linked.

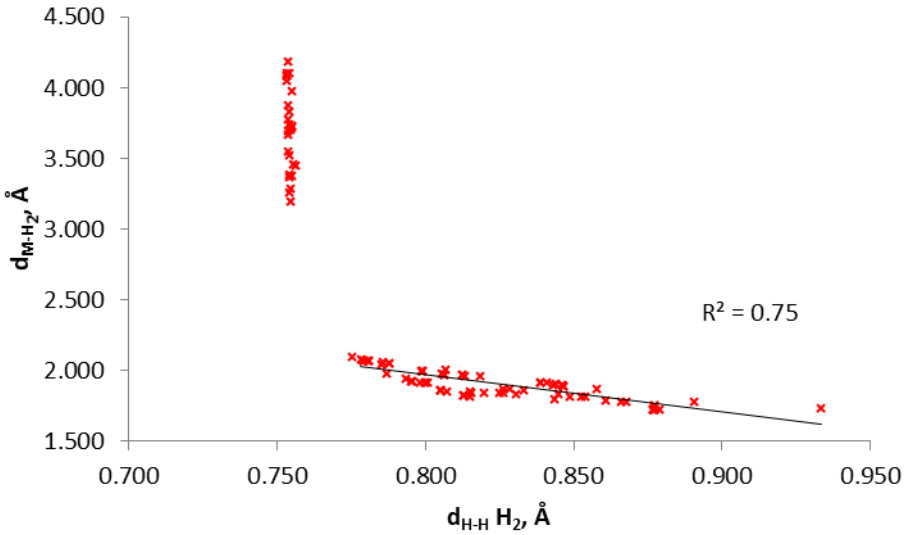

Figure 7. Correlation between $d_{H\text{-}H}$ H_2 and $d_{M\text{-}H2}$ for the H_2 on the 5 metal centre systems; Ti_5H_{15}, V_5H_{15}, and Cr_5H_{11}. This includes every H_2 detailed in Tables 6 and S2, although the R^2 value is for only the Kubas-bound H_2

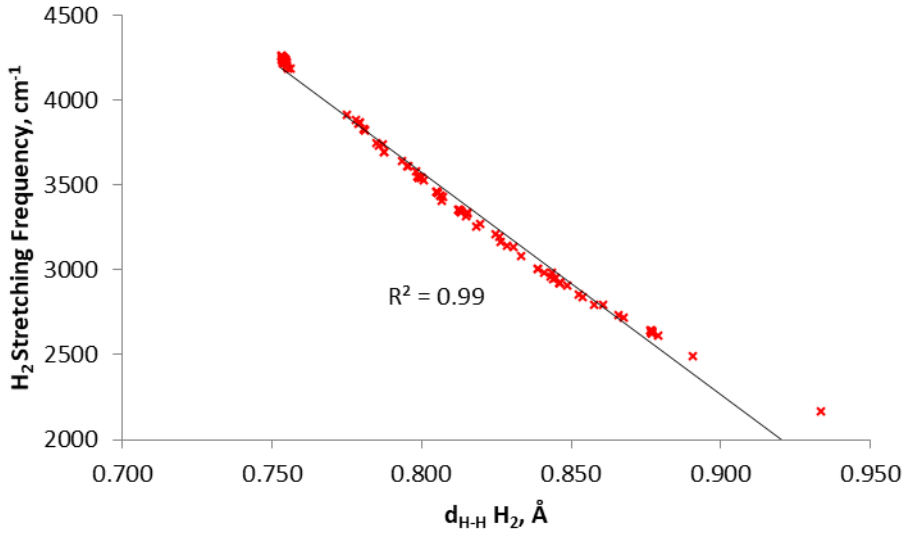

Figure 8. Correlation between $d_{H\text{-}H}$ H_2 and the stretching frequencies of H_2 for the H_2 on the 5 metal centre systems; Ti_5H_{15}, V_5H_{15}, and Cr_5H_{11}. This includes every H_2 detailed in Tables 6 and S2.

Comparisons with Our Previous Experimental and Computational Work

Our previous experimental work on MH_3[24-26] suggests that each system can bind between 1 and 2 H_2 per metal centre. This is apparent from the gravimetric adsorption, wt%, H_2 stored for each MH_3 system, and the Raman spectra. The experimental data for TiH_3 show 3.49 wt% H_2 at 140 bar and 298 K,[25] which is around 1 H_2 per metal centre, projected to be 5.8 wt% when phase pure, which is nearer to 2 H_2 per Ti. The Raman spectrum for H_2-loaded TiH_3 at 100 bar shows 3 different Kubas H_2 signals at around 3000 cm^{-1}, suggesting multiple binding site types and/or multiple H_2 bound to a metal centre; there is negligible physisorbed H_2 seen under these conditions. In our Ti_5H_{15} model we see a loading of 1.8 Kubas bound H_2 per metal centre, 6.6 wt%, a little above that seen experimentally but close to the projected maximum. When physisorbed H_2 are included we find a maximum loading of 10.6 wt%, 3.0 H_2 per metal centre, much greater than the ideal projected experimental absorption but, as noted, little physisorbed H_2 is seen experimentally. We calculate H_2 stretching frequencies at c. 3000 cm^{-1}, as seen experimentally. The experimental heats of adsorption rise as loading of H_2 is increased, and is projected to maximise at 32 kJ mol^{-1}, very close to the 37.1 kJ mol^{-1} we calculate for just the Kubas bound H_2. In general, then, there is good agreement between theory and experiment for this system.

The experimental data for VH_3 show a gravimetric storage of 5.8 wt% at 130 bar and 298 K, which is between 1 and 2 H_2 per metal centre[26]. This compares well with our calculated Kubas-like maximum; 1.4 H_2 per centre, 4.9 wt%, but is somewhat lower than the maximum including physisorption; 2.6 H_2 per centre, 8.8 wt%. The Raman spectrum for VH_3 under 100 bar of H_2 shows a weak signal at 4105 cm^{-1} attributed to physisorbed H_2 and has 3 other signals, assigned to Kubas-bound H_2, at 2770, 2929 and 3834 cm^{-1}. We find a range of

stretching frequencies from 3489 to 3641 cm^{-1} for Kubas-like H_2 along with stretches around 4200 cm^{-1} for physisorbed H_2. Hence the quantitative agreement between theory and experiment for the stretching frequencies is less good than for the Ti system, but qualitatively correct in finding both Kubas and physisorbed H_2. By contrast to TiH_3, the experimental enthalpy of H_2 adsorption is found to be only 0.52 kJ mol^{-1} for VH_3, much lower than from our calculations and also lower than that expected for room temperature Kubas binding. This has been attributed[28] to the material deforming under pressure and thus buffering the energy release of H_2 complexation, an effect not accounted for in our computational model. We return to this issue below. This discrepancy is not seen for the Ti case as the heat of adsorption given in that study is a linear extrapolation from much lower loading levels.

CrH_3 has a gravimetric storage of 5.08 wt% H_2 at 160 bar and 298 K which, again, suggests the material binds between 1 and 2 H_2 per metal centre.[24] We calculate only 3.6 wt% of H_2 from Kubas binding, rather lower than experiment. When the calculated physisorbed H_2 are included we find a gravimetric weight percentage of 8.1 wt%, now well above the experimental value. These data suggest that, like VH_3, experiment is measuring both Kubas and physisorbed H_2. Consistent with this, the experimental Raman spectrum shows signals at around 4100 to 4200 cm^{-1}, also seen in our models when physisorbed H_2 are considered. Raman spectroscopy also finds 3 signals at 2789, 2922 and 3188 cm^{-1} attributed to H_2 complexation; we calculate a range of stretching frequencies from 2625 to 3461 cm^{-1} for Kubas-like H_2 suggesting we are finding similar binding motifs. As with VH_3, the Cr system is found experimentally to have a very low adsorption enthalpy, 0.37 kJ mol^{-1}, whilst still maintaining H_2 binding properties at room temperature. This much lower than expected

value, which again disagrees with our HBE data, is also attributed to pressure causing the system to distort, buffering the binding energy[28].

We have previously reported computational work on the H_2 binding properties of hydrazide linked systems of Ti, V and Cr,[28,29] studying both M(II) and M(III) oxidation states. The M(II) hydrazide monomers,[28] with various ancillary ligands including trimethylsilylmethyl, hydrides, hydrazides, and THF, can bind between 1 and 3 H_2 per metal centre. There is a trend across all the systems in which Cr binds fewer H_2 than V which in turn binds fewer than Ti; this is the same as we report above for H_2 Kubas bound to MH_3. The M(II) hydrazide systems show Kubas like binding, although there is no clear trend as to which metal has the strongest binding; the trends are dependent on the ancillary ligand present. The dimers of the M(II) hydrazide systems also show no clear binding energy trends across the series, but still display clear Kubas H-H bond extension and stretching frequencies.

The trend to fewer Kubas bound H_2 across the series is also present in the M(III) hydrazide dimers,[29] and once again there is no strong HBE trend at the various loading levels considered. The energies we found for the fully hydrazide based M(III) systems are lower than we observe for the present hydride systems. However, when a hydride is introduced to the Ti(III) hydrazide system there is a large increase in the HBE to a level similar to our hydrides, -47.83 kJ mol^{-1}.

As with the MH_3 systems, the structure of these hydrazine systems is thought to distort under pressure of H_2, buffering the energy gain of H_2 complexation. We previously tested this effect computationally[28] by determining the energy differences between the base structures before and after the addition of H_2, finding a destabilising change in the energy per H_2 of between 20.5 and 37.2 kJ mol^{-1} for V(III) and between 42.2 and 44.6 kJ mol^{-1} for

Cr(II). When similar data are obtained for the model MH_3 systems under consideration in this study we find an energy difference per H_2 in the pentameric base structures before and after attaining maximum Kubas loading of 8.1 kJ mol^{-1} for Ti_5H_{15}, 12.6 kJ mol^{-1} for V_5H_{15} and, 17.7 kJ mol^{-1} for Cr_5H_{11}, which at least qualitatively suggests that a similar buffering/flexing mechanism to that previously proposed is possible for these materials. Since a real world structure would require reordering of bonds in 3 dimensions rather than only 2 dimensions in the modelled pentamers, greater reorganization energies would be expected in reality.

Conclusions

In this contribution, we have presented quantum chemical computational evidence that mono- and multi-metallic models of MH_3 (M=Ti, V, and Cr) can all employ Kubas-like complexation to bind dihydrogen *via* interaction between the metal d orbitals and the H_2 σ and σ* orbitals. All of the models show a large affinity for H_2, with binding energies at the upper end of those expected for such an interaction; each also shows the Kubas motif of extended H_2 bond lengths. The experimental energies are much lower than those we calculate, the projected HBE for TiH_3 is of the same magnitude as the calculated value. This energy discrepancy is attributed to flexing of the macro structure, which buffers the energy released by hydrogen binding.

The amount of H_2 found to bind to these systems *via* the Kubas mechanism is consistent with our previous experimental data; between 1 and 2 H_2 per metal centre. When all our physisorbed H_2 are included we find that our models bind more H_2 than the experimental systems, with TiH_3 binding as many as 3 H_2 per centre. Qualitatively, however, our models agree well with experiment. Combining data from experiment and computation, we conclude that TiH_3 binds almost exclusively *via* the Kubas interaction, whereas VH_3 and CrH_3 bind using both Kubas and physisorption. It is likely the extent of the latter which is responsible for the quantitative differences between experiment and theory for the amount of H_2 that can bind to VH_3 and CrH_3, most likely arising from the limitations of a small molecular cluster representation of an extended system.

It has been shown across our previous work, and in this study, that the early transition metals from Ti to Mn can bind H_2 via the Kubas interaction. We have seen trends across these studies that show that when Ti binds H_2 it achieves a greater maximum loading than the other transition metals across the series. However, the HBEs do not correlate well with

the maximum loading throughout; similar trends in binding energies have been seen in this work and our previous systems.[28, 29]

Consideration of the pentameric models suggests that VH_3 would provide the best practical alternative from a cost/performance perspective as it binds H_2 the most strongly, while also supporting a significant number of H_2 per metal atom, with vanadium costing significantly less than chromium or titanium. The reason that experimental studies have yielded lower values in all three cases is likely related to the lack of convenient metal alkyl precursors and overall control over the decomposition of the metal alkyl into a porous metal hydride with maximum diffusion characteristics and available binding sites. For this reason continued synthetic efforts into this exciting new class of materials are warranted.

Acknowledgments

The authors acknowledge Hydro Quebec and the University of Manchester for funding. We also thank the Computational Shared Facility (CSF) at the University of Manchester for computational resources and associated support services.

References

1. P. Jena. *Journal of Physical Chemistry Letters*, **2011**, *2*, 206-211.
2. M. Balat, *International Journal of Hydrogen Energy*, **2008**, *33*, 4013–4029.
3. J. Ren, H. W. Langmi, B. C. North, M. Mathe, *International Journal of Energy Research*, **2015**, *39*, 607.
4. R. von Helmolt, U. Eberle, *Journal of Power Sources*, **2007**, *165*, 833.
5. N.A.A. Rusman, M. Dahari, *Int. J. Hydrogen Energy*, **2016**, *41*, 12108.
6. L. Schlapbach, A. Züttel. *Nature*, **2001**, *414*, 353.
7. D. Durbin, C. Malardier-Jugroot, *Int. J. Hydrogen Energy,* **2013**, *38*, 14595.
8. J. M. Simmons, T. Yildirim, A. Hamaed, D. M. Antonelli, M. I. Webb and C. J. Walsby,*Chem. Eur. J.*, **2012** *18*, 4170-4173
9. M. Dincă, A. F. Yu, & J. R. Long, *Journal of the American Chemical Society*, **2006,** *128*, 8904–8913.
10. M. Dincă, A. F. Yu, & J. R. Long, *Journal of the American Chemical Society*, **2005,** *127*, 9376–9377.
11. M. P. Suh, H. J. Park, T. K. Prasad, & D. Lim, *Chemical Reviews*, **2012**, *112*, 782–835.
12. A. G. Wong-Foy, A. J. Matzger & O. M. Yaghi, *Journal of the American Chemical Society*, **2006**, *128*, 3494–3495.
13. B. Sakintuna, F. Lamari-Darkrim, M. Hirscher, *International Journal of Hydrogen Energy*, **2007**, *32*, 1121
14. B. Bogdanović, M. Schwickardi, *Journal of Alloys and Compounds*, **1997**, *253*, 1-9
15. G. J. Kubas, *Chem. Rev.,* **2007**, *107*, 4152.
16. G. J. Kubas, *Journal of Organometallic Chemistry*, **2009**, *694*(17), 2648–2653.
17. , T. K. A. Hoang, & D. M. Antonelli, *Advanced Materials*, **2009**, *21*(18), 1787–1800.
18. G. J. Kubas, C. J. Unkefer, B. I. Swanson & E. Fukushima, *Journal of the American Chemical Society*, **1986**, *108*(22), 7000–7009.
19. P. Atkins and D. Shriver, Inorganic Chemistry, **2010**, Oxford University Press, 5th Ed.
20. C. V. J. Skipper, A. Hamaed, D. M. Antonelli, & N. Kaltsoyannis, *Dalton Transactions*, **2012**, *41*(28), 8515–23.
21. C. V. J. Skipper, T. K. A. Hoang, D. M. Antonelli, & N. Kaltsoyannis, *Chem. Eur. J.*, **2012**, *18*(6), 1750–60.
22. A. Hamaed, H. Van Mai, T. K. A. Hoang, M. Trudeau, & D. Antonelli, *The Journal of Physical Chemistry C*, **2010**, *114*(18), 8651–8660.
23. C. V. J. Skipper, A. Hamaed, D. M. Antonelli, & N. Kaltsoyannis, *Journal of the American Chemical Society*, **2010**, *132*(48), 17296–305.
24. L. Morris, M. L. Trudeau, D. Reed, D. Book, D. M. Antonelli, *Phys. Chem. Chem. Phys.*, **2015**, *17,* 9480.
25. T. K. A. Hoang, L. Morris, D. Reed, D. Book, M. L. Trudeau, & D. M. Antonelli, *Chemistry of Materials*, **2013**, *25*, 4765–4771.
26. L. Morris, L. A. C. Smith, M. L. Trudeau, D. M.Antonelli *J. Phys. Chem C*,.**2016**, *120*, 11407-11414.
27. L. Morris, J. J. Hales, M. L. Trudeau, P. Georgiev, J. P. Embs, J. Eckert, N. Kaltsoyannis and D. M. Antonelli, *Energy and Environmental Science*, **2019**, DOI: 10.1039/c8ee02499e
28. C. V. J. Skipper, D. M. Antonelli, & N. Kaltsoyannis, *The Journal of Physical Chemistry C*, **2012**, *116*(36), 19134–19144.
29. C. V. J. Skipper, A. Hamaed, D. M. Antonelli, & N. Kaltsoyannis, *Dalton Transactions*, **2012**, *41*(28), 8515–23.
30. C. V. J. Skipper, T. K. A. Hoang, D. M. Antonelli, & N. Kaltsoyannis, *Chem. Eur. J.*, **2012**, *18*(6), 1750–60.
31. J. P. Perdew, K. Burke, M. Erzerhof, *Physical Review Letters*, **1996**, *77*, 3865.
32. J. P. Perdew, K. Burke, M. Erzerhof, *Physical Review Letters*, **1997**, *78*, 1396.
33. S. Grimme, J. Antony, S. Ehrlich, H. Krieg, *The Journal of Chemical Physics*, **2010**, *132*, 154104.
34. A. J. H. Wachters, *The Journal of Chemical Physics*, **1970**, *52*(3), 1033.
35. P. J. Hay, *The Journal of Chemical Physics*, **1977**, *66*(10), 4377.
36. A. D. McLean, & G. S. Chandler, *The Journal of Chemical Physics*, **1980**, *72*(10), 5639.
37. R. Krishnan, J. S. Binkley, R. Seeger, & J. A. Pople, *The Journal of Chemical Physics*, **1980**, *72*(1), 650.
38. E. Tsivion, J. R. Long, & M. Head-Gordon, *Journal of the American Chemical Society*, **2012**, *136*, 17827–17835.
39. R. C. Lochan, & M. Head-gordon, *Physical Chemistry Chemical Physics*, **2006**, *8*, 1357–1370.

40. M. Kocman, P. Jurečka, M. Dubecký, M. Otyepka, Y. Cho and K. S. Kim, *Physical Chemistry Chemical Physics,* **2015**, *17*, 6423.
41. J. Gebhardt, F. Viñes, P. Bleiziffer, W. Hieringer, A. Görling, *Physical Chemistry Chemical Physics,* **2015**, *16*, 5382–5392.
42. A. Mavrandonakis, K. D. Vogiatzis, A. D. Boese, K. Fink, T. Heine, W. Klopper. *Inorganic Chemistry*,**2015**, 54, 8251–8263.
43. M. Manadé, F. Viñes, A. Gil, F.Illas. *Physical Chemistry Chemical Physic*s, **2018**, *20*, 3819–3830.
44. Gaussian 09, Revision D.01, M. J. Frisch, G. W. Trucks, H. B. Schlegel, G. E. Scuseria, M. A. Robb, J. R. Cheeseman, G. Scalmani, V. Barone, B. Mennucci, G. A. Petersson, H. Nakatsuji, M. Caricato, X. Li, H. P. Hratchian, A. F. Izmaylov, J. Bloino, G. Zheng, J. L. Sonnenberg, M. Hada, M. Ehara, K. Toyota, R. Fukuda, J. Hasegawa, M. Ishida, T. Nakajima, Y. Honda, O. Kitao, H. Nakai, T. Vreven, J. A. Montgomery, Jr., J. E. Peralta, F. Ogliaro, M. Bearpark, J. J. Heyd, E. Brothers, K. N. Kudin, V. N. Staroverov, R. Kobayashi, J. Normand, K. Raghavachari, A. Rendell, J. C. Burant, S. S. Iyengar, J. Tomasi, M. Cossi, N. Rega, J. M. Millam, M. Klene, J. E. Knox, J. B. Cross, V. Bakken, C. Adamo, J. Jaramillo, R. Gomperts, R. E. Stratmann, O. Yazyev, A. J. Austin, R. Cammi, C. Pomelli, J. W. Ochterski, R. L. Martin, K. Morokuma, V. G. Zakrzewski, G. A. Voth, P. Salvador, J. J. Dannenberg, S. Dapprich, A. D. Daniels, Ö. Farkas, J. B. Foresman, J. V. Ortiz, J. Cioslowski, and D. J. Fox, Gaussian, Inc., Wallingford CT, 2009.
45. Gaussian 16, Revision B.01, M. J. Frisch, G. W. Trucks, H. B. Schlegel, G. E. Scuseria, M. A. Robb, J. R. Cheeseman, G. Scalmani, V. Barone, G. A. Petersson, H. Nakatsuji, X. Li, M. Caricato, A. V. Marenich, J. Bloino, B. G. Janesko, R. Gomperts, B. Mennucci, H. P. Hratchian, J. V. Ortiz, A. F. Izmaylov, J. L. Sonnenberg, D. Williams-Young, F. Ding, F. Lipparini, F. Egidi, J. Goings, B. Peng, A. Petrone, T. Henderson, D. Ranasinghe, V. G. Zakrzewski, J. Gao, N. Rega, G. Zheng, W. Liang, M. Hada, M. Ehara, K. Toyota, R. Fukuda, J. Hasegawa, M. Ishida, T. Nakajima, Y. Honda, O. Kitao, H. Nakai, T. Vreven, K. Throssell, J. A. Montgomery, Jr., J. E. Peralta, F. Ogliaro, M. J. Bearpark, J. J. Heyd, E. N. Brothers, K. N. Kudin, V. N. Staroverov, T. A. Keith, R. Kobayashi, J. Normand, K. Raghavachari, A. P. Rendell, J. C. Burant, S. S. Iyengar, J. Tomasi, M. Cossi, J. M. Millam, M. Klene, C. Adamo, R. Cammi, J. W. Ochterski, R. L. Martin, K. Morokuma, O. Farkas, J. B. Foresman, and D. J. Fox, Gaussian, Inc., Wallingford CT, 2016.